Astron. Astrophys. 327, 689–698 (1997)

ASTRONOMY AND ASTROPHYSICS

The rich molecular content of OH 231.8+4.2

C. Sánchez Contreras[1,2], **V. Bujarrabal**[1], **and J. Alcolea**[1]

[1] Observatorio Astronómico Nacional (IGN), Apartado 1143, E-28800 Alcalá de Henares, Spain ([sanchez,bujarrabal,j.alcolea]@oan.es)
[2] Departamento de Astrofísica, Facultad C. Físicas, Universidad Complutense, E-28040 Madrid, Spain

Received 13 March 1997 / Accepted 24 June 1997

Abstract. We have carried out maps of microwave lines of 8 different molecules (^{12}CO(2-1 and 1-0), ^{13}CO(2-1 and 1-0), SiO(5-4), HCO$^+$(1-0), $SO_2(10_{0,10}$-$9_{1,9})$, CS(5-4), HCN(1-0) and HNC(1-0)) in OH 231.8+4.2, a protoplanetary nebula that shows a particularly rich molecular emission. Confirming previous observations, the total molecular extent is comparable to the optical image and the lines show a total velocity range $\sim$ [$-$80:+250] km s^{-1} (LSR), due to a high-velocity flow in the axial direction. The observed transitions show a practically constant velocity gradient, $\sim$ 6 km s^{-1} per arcsec, in the direction of the polar axis. All the observed molecular lines (except for HCO$^+$) show similar emission features: an intense component in the velocity range [+10:+55] that comes from the nebula center, and weaker wing emission originating in the lobes, that appear fragmented in several gas components flowing at high velocity in the axial direction. HCO$^+$, remarkably, does not show a dominant central feature, its emission being dominated by the contribution of the fast clumps. From the intensity ratio of the ^{13}CO transitions, we have estimated that the CO excitation remains practically constant in the whole nebula, the rotational temperature showing a low value, $\sim$ 10 K. We have also calculated the mass, momentum and molecular abundances in the different components of the nebula. We estimate a total molecular mass in the envelope of 0.5$-$1 $M_\odot$, and at least 0.2 $M_\odot$ are axially flowing at velocities (with respect to the systemic one) larger than 40 km s^{-1}. It is argued that this material corresponds to a large fraction of the envelope ejected in the previous AGB phase, after being accelerated by interaction with the fast post-AGB jets. We stress that the high value of the measured axial momentum cannot be explained by radiation pressure, a different mechanism for the release of kinetic momentum by the star must be at work. The abundances of CS, HNC and HCN are found to be practically constant across the nebula. SO_2 is more abundant in the south lobe, while SiO shows the opposite behavior, confirming the asymmetry of the source with respect to the equatorial plane. The HCO$^+$ abundance is found to be much higher in the axial flow than in the central component of the nebula, as expected in view of its intensity distribution. We suggest that this molecule (and probably SiO) is efficiently formed in the lobes of OH 231.8+4.2 by shock-induced reactions.

Key words: circumstellar matter – stars: AGB and post-AGB – stars: abundances – stars: individual: OH 231.8+4.2 – radio lines: stars

1. Introduction

OH 231.8+4.2 (also known as OH0739$-$14, the Calabash Nebula, and the Rotten Egg Nebula; hereafter OH 231.8) is one of the best studied protoplanetary nebulae (PPNe). Its relative proximity and large angular extent are important advantages for the analysis of the complex dynamics often present in this kind of objects. In the visible, OH 231.8 shows a clear axial symmetry with two lobes at both sides of the central star, two collimated streamers and an obscuring ridge between the lobes (Reipurth 1987, Kastner et al. 1992, and references therein). The axis of the nebula is oriented almost in the north-south direction; the length of the nebula along this axis is about 50″. The size in the perpendicular direction is $\lesssim$ 10″ in most of the nebula, except for a somewhat larger size in the southern extension. The inclination of the axis with respect to the plane of the sky is quite well known, $i \sim 40^\circ$, with the south lobe further away (see Shure et al. 1995, Kastner et al. 1992). The southern lobe is about twice more extended than the northern one, being ended by a remarkable bow-shaped feature. Herbig-Haro objects are observed at the front of the lobes, which are probably related to shocks caused by wind interaction, a phenomenon thought to often take place in the post-AGB phase (Cohen et al. 1985). Optical spectroscopy indicates that the spectral type of the hidden central star is M9 III (Cohen, 1981). However, the blue excess detected in its spectrum could suggest the presence of a hotter companion.

The distance to OH 231.8, particularly well known for a PPN, is of the order of 1300/tan(i) pc, i.e. $\sim$ 1500 pc for $i = 40^\circ$, as derived from the comparison of phase lag and angular extent measurements in both OH maser emission and IR continuum (Bowers and Morris 1984, Kastner et al. 1992). Kastner et al. estimates that errors in this distance should not exceed $\pm$ 400 pc. For this distance, the total extent of the nebula is $\sim 10^{18}$ cm and the total luminosity is $\sim 10^4$ $L_\odot$.

OH 231.8 is also a remarkable molecular line emitter. The ^{12}CO line profiles are found to be wide, between about -80 and +250 km s^{-1} LSR, with an intense central component $\sim$ 40 km s^{-1} wide, as well as weaker wings (Alcolea et al. 1996). These authors conclude that the total mass probed by CO is $\sim 0.5-1\ M_{\odot}$; probably it is the dominant component of the nebular material and was ejected during the post-AGB phase. A compact central clump that shows a low expansion velocity ($\sim$ 20 km s^{-1}), contains $\gtrsim 0.4\ M_{\odot}$. This part of the circumstellar envelope does not seem to be affected by wind interaction during the evolution from the AGB phase toward planetary nebula. The red and blue wings arise respectively from the south and north parts of the nebula. It is remarkable that the strong velocity gradient in the axial direction does not practically vary along the whole nebula, $\sim$ 6 km s^{-1} per arcsec, leading to a flow (deprojected) velocity as high as 330 km s^{-1}. The present high velocities are probably due to shock interaction with the fast, bipolar post-AGB ejections. The molecular mass that axially flows at more than 40 km s^{-1} is very large, at least $\sim 0.1\ M_{\odot}$, following Alcolea et al.

OH 231.8 is also a peculiar OH maser emitter. The OH lines are less wide than those of CO, occupying between -15 and +80 km s^{-1} LSR. The OH source has a extent of $\sim 10''$ in the axial direction and $\sim 6''$ in the perpendicular one, being centered on the star position (Morris et al. 1982). OH 231.8 also presents strong H_2O and SiO maser emission. Such maser emission is only observed in oxygen-rich objects, so we conclude that OH 231.8 is very probably O-rich. However, this source is unusual in its chemistry because of the relatively strong emission from carbon-bearing molecules like HCN, HNC and CS, normally indicators of a carbon-rich chemistry. The strong emission of sulfur-containing molecules like H_2S, SO_2 and SO is also remarkable (Ukita and Morris 1983, Omont et al. 1993). Up to date, the molecular abundances calculated for OH 231.8 are only average values that do not account for the possible differences between the various velocity components of the nebula, and must mainly correspond to the central clump. The abundance and excitation state of the diffuser regions rapidly flowing along the axis was up to now practically unknown. The purpose of this paper is to improve our knowledge on the mass distribution and the chemical composition of OH 231.8, particularly in the axial gas flow.

2. Observations

We have performed maps of several molecular lines in OH 231.8+4.2 using the IRAM-30 m MRT at Pico de Veleta (Granada, Spain) in two observing sessions, October 1995 and November 1996. Three SiS receivers working in the 3, 2 and 1.3 mm bands were used at the same time to observe simultaneously different spectral lines (^{12}CO(2-1),^{13}CO(2-1), SiO(5-4) and CS(5-4) at λ = 1.3 mm; $SO_2(10_{0,10}$-$9_{1,9})$ at λ = 2 mm; and ^{12}CO(1-0), ^{13}CO(1-0), HCO$^+$(1-0), HCN(1-0) and HNC(1-0) at λ = 3 mm). The receivers were always tuned in SSB mode (LSB), with typical system temperatures of $\sim 1000-2300$ K at λ = 1.3 mm, $\sim$ 1100 K at λ = 2 mm and $\sim$ 500 K at λ = 3 mm (in units of $T_{\rm mb}$, see below). Each receiver IF was connected to a 1 MHz resolution filter bank. We have observed ^{12}CO emission from OH 231.8 towards 47 positions fully covering the extent of the nebula. Points are separated by $\sim 7''$ (see Fig. 2). The data obtained in the first observing session for ^{12}CO have been previously reported by Alcolea et al. (1996). We have observed again the ^{12}CO J=2$-$1 line in order to improve the quality of the maps and we present here the final results. ^{13}CO (1-0) and SO_2 emission have also been observed at a large number of points (21) over the whole nebula. For the rest of the molecular lines, we observed $\sim 8-13$ points along a cross with its largest arm probing the nebular axis.

All the data presented here are calibrated in units of Main Beam Rayleigh-Jeans equivalent Antenna Temperature, $T_{\rm mb}$, using the chopper wheel method by observing hot (ambient) and cold loads (liquid nitrogen). In addition, observations of the well known evolved star CW Leo (IRC+10216) were used to check the calibration of our data with that of previous works.

Weather conditions were quite good for most observations, with zenith opacities at 230 GHz ranging from 0.3 to 0.6 in October 1995 and from 0.08 to 0.3 in November 1996. The pointing of the telescope was verified every about two hours by observing (cross-scanning) continuum sources close in the sky to our target. In order to minimize the effects of possible receiver missalignments, the pointing was done using the 1.3 mm receiver, since it has the narrowest beam (about 13$''$ including the effects of pointing errors during the observations). Absolute pointing errors at λ = 1.3 mm smaller than $\sim 3''$ are expected. Receiver alignment was checked by simultaneously observing at all wavelengths strong continuum sources (mainly planets). The pointing discrepancies between the 1.3 and 3 mm receivers were found to be much smaller (between $\sim\ 2-4''$) than the HPBW at 3 mm (22$''$). The missalignment between the 1.3 and 2 mm was also very small ($\sim\ 2.5''$, to be compared with a HPBW of $\sim\ 16''$).

3. Results

We show in Fig. 1 the spectra at the nebula center for all the observed molecular transitions. The adopted coordinates for the central position are: (B1950) 07:39:59.0, -14:35:41. We see that, except for HCO$^+$, the line profiles are similar, with a relatively narrow component (between $\sim$ 10-55 km s^{-1} LSR) centered at $\sim$ 33 km s^{-1} LSR that dominates the emission, and two weaker wings. The central spectral component arises from the central compact condensation while the wings, that reach very high velocities, arise from the nebula lobes. HCO$^+$, contrarily, shows a flat line profile between ~ -30 and +80 km s^{-1} LSR, the emission from the wings in this velocity range being as intense as the central spectral component. We can see in this spectrum a feature between -80 and -30 km s^{-1} LSR also visible at other adjacent positions (see below).

In Fig. 2 we can see the spatial distribution of the ^{12}CO J=2$-$1 velocity integrated intensity from OH 231.8. A sketch of the source appearance at optical wavelengths, the beam half-maximum contour and the observed positions are also repre-

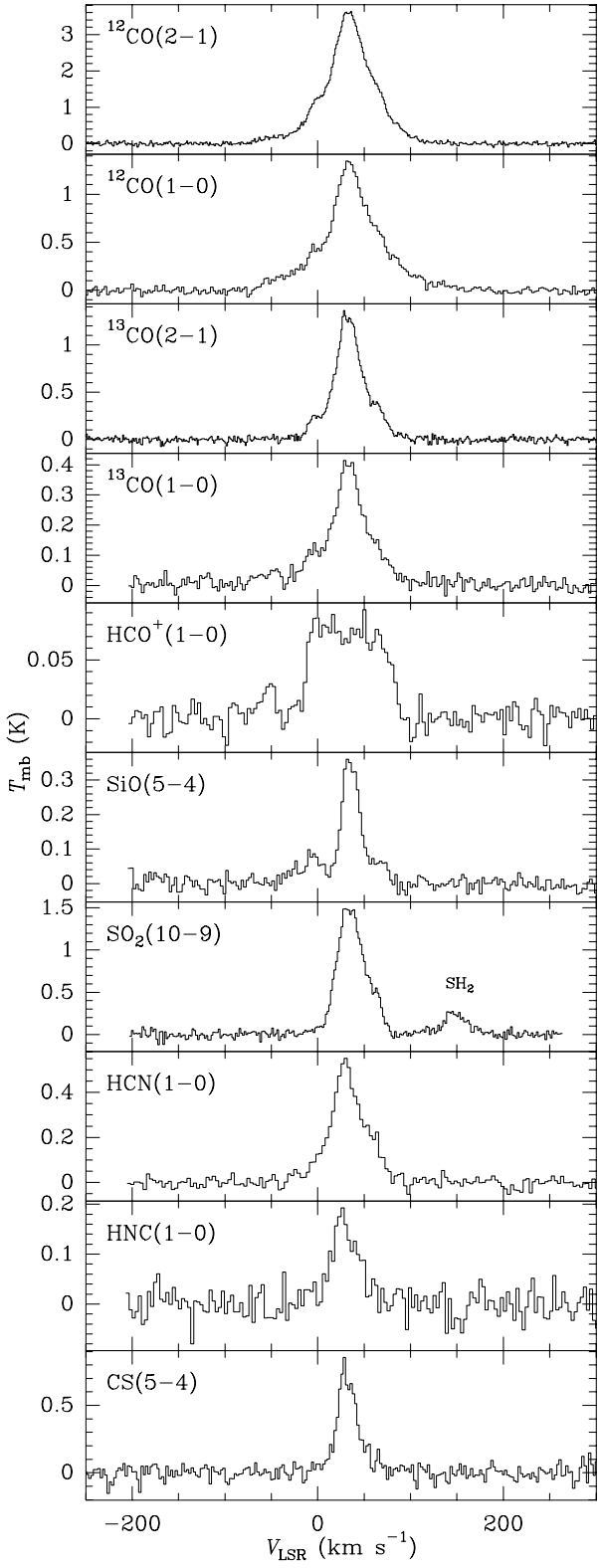

Fig. 1. Central position spectra of the molecular transitions observed in OH 231.8 in units of main-beam temperature and projected velocity (LSR).

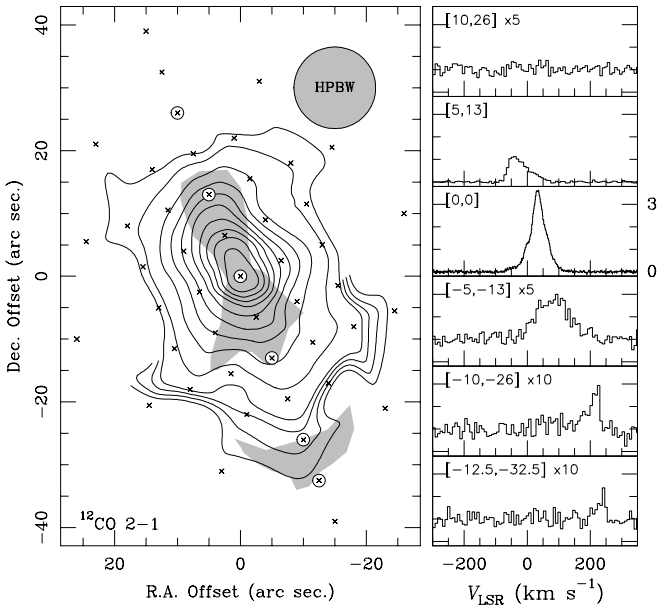

Fig. 2. Map of the integrated intensity of the ^{12}CO J=2−1 line and spectra for selected points along the symmetry axis. For the spectra, east and north offsets are indicated within square brackets. Contours are 2, 3, 4, 5 and 10 to 90 by 10% of the maximum (219 K km s^{-1}). The observed points are indicated with small crosses, the encircled ones are the positions for which the spectra are shown. The beam size and a sketch of the source in the visible is also shown in light grey. Central coordinates: (B1950) 07:39:59.0, −14:35:41.

sented in this figure. The total deconvolved extent along the nebula symmetry axis is about 50″, comparable to that of the optical image. In the right panels we see the spectra of this line in representative points along the axis. Note that the quality of the ^{12}CO J=2−1 map of our first observations (Alcolea et al. 1996) has been improved by adding the data of a second observing period.

We show in Fig. 3 the displacement of the emitting gas along the axis for different LSR velocity intervals: I1 [−80:−30], I2 [−30:+10], I3 [+10:+55], I4 [+55:+80], I5 [+80:150], and I6 [+150:250] (ranges in km s^{-1}, see right-top corners in the figure). These velocity intervals are similar to those chosen by Alcolea et al. (1996) and correspond to different components that can be found in both our line profiles and spatial intensity distributions (see Figs. 1 and 4, and discussion below). We confirm that the emission from the top, bottom and center of the nebula takes place at very different velocities, which shows that the features detected in the different map positions correspond to independent emitting gas. It is also remarkable that the clump with the highest (positive) velocity lies on the southern bow-like structure of the nebula in the visible. For cuts along the direction perpendicular to the nebular axis, the deconvolved size of the CO emission at half maximum intensity is always $< 10''$. This is in agreement with the small extent of the nebula in OH maser emission and in the visible, except for the southernmost part: the larger extent of the optical emission in this region has no clear

counterpart in the compact high velocity clump observed in CO. No velocity gradient is detected in the direction perpendicular to the nebula axis.

In Fig. 4 we show the velocity-position diagrams along the symmetry axis of the nebula for the ten observed transitions. The spectral resolution is ~ 11 km s^{-1}. The maps are distributed in two columns according to their spatial resolution, $\sim 13-16''$ for the first column and $\sim 22-28''$ for the second one. The apparently larger extent of the molecular emission in the second column is then an effect of the lower spatial resolution. We can see, looking at the velocity-position maps, that there is a clear velocity gradient along the symmetry axis. By virtue of its large abundance and intense emission, ^{12}CO remains the best tracer of the nebular material, showing the largest spatial size and better defining the different components of the molecular envelope. The velocity gradient, determined from the ^{12}CO J=2−1 map, is approximately constant (~ 6 km s^{-1} per arcsec), the highest expansion velocity being associated to the southernmost part of the nebula. Taking into account the inclination of the nebula axis with respect to the plane of the sky, $\sim 40°$, we deduce that the molecular gas is flowing with velocities (relative to that of the central core) up to 180 km s^{-1}, in the north lobe, and up to 330 km s^{-1}, in the southern one. We can also see in Fig. 4 that the velocity-position maps appear fragmented, showing different spectral features located at clearly separated positions along the nebula axis (this structure approximately corresponds to the velocity ranges, I1 to I6, that for simplicity we are considering in some calculations).

Note that the same velocity gradient and nebula fragmentation seem to be present in all the observed transitions. They clearly appear in the ^{13}CO, SiO and HCO$^+$ maps. We remark that the signal to noise ratio is poor in the the CS, SO_2, HCN and HNC wings. Nevertheless, also in these cases, we find emission from the clumps with velocities between ~ -30: +10 and $\sim +55$: +80 km s^{-1} LSR at the position expected from the axial velocity gradient found for the other molecules. We can better see this in Fig. 5, which shows the variation along the symmetry axis of the integrated intensity in representative (projected) velocity ranges. It is clear that the red/blue wings are shifted toward the south/north lobe for all the molecular transitions. Note that there is probably emission of CS, HCN and HNC also between −80 and −30 km s^{-1} LSR (see Fig. 4). These features are located at the positions that correspond to the velocity gradient of the molecular gas, so we think that they are real. We must note that the J=1−0 HCN transition shows hyperfine components separated by ~ 11 km s^{-1}, which can degrade the effective spectral resolution of our velocity-position map (Figs. 4 and 5). However, this effect could be only important in the central part of the diagram, due to the very large velocity gradient of the nebula.

It is remarkable that the central clump dominates the emission for all the molecular transitions except for HCO$^+$. In Fig. 4 we clearly see that a relative minimum of emission appears at the central velocity interval while the other molecules clearly show the most intense emission at this velocity range. This behavior cannot be due to selfabsorption, since in circumstellar envelopes selfabsorption always appears at the negative-velocity edge of the line profile. Indeed, the very weak HCO$^+$ emission suggests a low optical depth, although we must note that this low intensity can also be due to a strong clumpyness. It seems that the bulk of the HCO$^+$ emission originates at the nebula lobes, where the gas is flowing faster because of the wind interaction. As we will discuss in Sect. 5, the molecular abundance of HCO$^+$ in OH 231.8 could be enhanced by shock-induced reactions, explaining the peculiar emission of this molecule. We tentatively detect a similar behavior for the HNC emission. The most intense component appears slightly shifted in velocity and position with respect to the dominant features of other lines, although this shift is compatible with the general velocity gradient. However the low signal to noise ratio in the HNC maps prevents to extract definitive conclusions.

The fragmentation found in the velocity-position maps of the observed molecules shows that the molecular envelope of OH 231.8 is formed by several components. The outer features with large expansion velocities, in the ranges [−80,−30] and [+150,+250], very probably correspond to independent condensations well separated from the rest (inner part) of the nebula. Other components, particularly those corresponding to the ranges [−30,+10] and [+55,+80], stand out from the different intensity distribution of certain molecules, like HCO$^+$ and SiO. They could perhaps represent regions of peculiar chemistry.

4. Mass, momentum and molecular abundances in OH 231.8+4.2

4.1. Calculation procedures and assumptions

We have calculated the mass and momentum of the clumps present in OH 231.8 and the abundances of the observed species. Some assumptions about the morphology and gas distribution in the source and the excitation conditions are needed. OH 231.8 does not show spherical symmetry but, as usually occurs for PPNe, a bipolar appearance. Moreover from our data we find that a clumpy structure is present in this nebula. For simplicity, we have defined six separated clumps, the central one that presents no axial velocity and presumably expands in a spherically symmetric way, and five kinematically independent regions of emitting gas flowing along the symmetry axis. The projected velocity ranges in km s^{-1} associated to the different clumps are the same used in Figs. 3 and 5 (see Sect. 3), I1 to I6. The source is found to be asymmetric about the system's equatorial plane. The I1 and I2 intervals are associated to the north lobe and the I4, I5 and I6 to the southern one. I3 is central spectral feature. We suppose that the clumps are homogeneous, i.e. molecular abundances do not vary inside the same clump. However, a change in the abundances from one emitting region to another is allowed.

We will assume that the ^{13}CO lines are optically thin. This is supported by the high difference between the observed ^{12}CO and ^{13}CO intensities, in spite of the expected similar excitation of both molecules. In fact both molecules are close to be thermalized for the density values, $\sim 10^4 - 10^5$ cm^{-3}, that correspond to the mass we will derive below. If the excitation of the lines

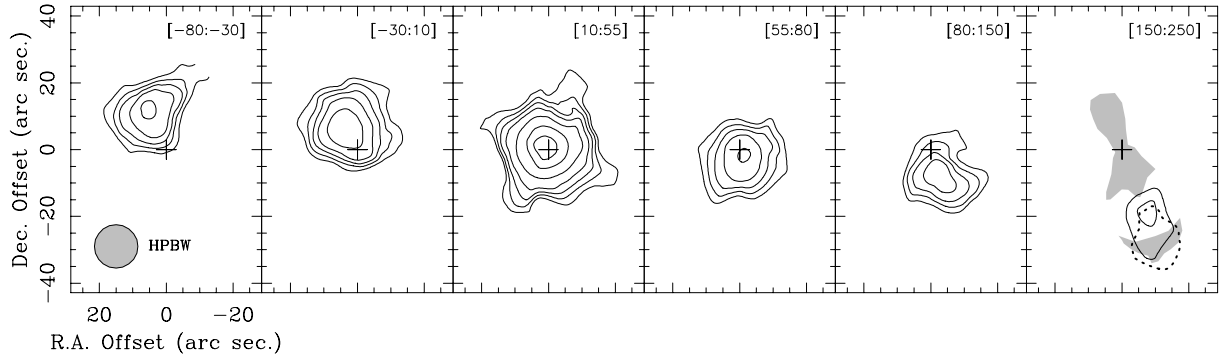

Fig. 3. Maps of the ^{12}CO J=2−1 integrated intensity in representative velocity ranges. The velocity intervals (km s^{-1} LSR) are indicated in the upper-right corners. Levels are 5 8.5 13 20 35 65 and 105 K km s^{-1}. In the last panel we also show a sketch of the nebula in the visible and the contour at half maximum of the integrated intensity for the interval [220:250] km s^{-1}(dashed line). Central coordinates: (B1950) 07:39:59.0, −14:35:41.

of both species is similar and the ^{12}CO lines are opaque, we can deduce the ^{13}CO line opacities. We so find from the ^{12}CO/^{13}CO intensity ratio (see Fig. 6) that the opacities of the ^{13}CO lines are $\tau(2-1) \sim 0.4$ and $\tau(1-0) \sim 0.3$, at the central velocities (and much smaller at other velocities). For these opacity values, the assumption of optically thin emission for the J=1−0 line, made below for the estimation of the nebular mass, would lead to an underestimation of the central clump mass of (only) 15%. Note from Fig. 6 that a strong opacity effect is expected in the ^{12}CO line core.

We will assume that the excitation temperature is the same in the CO low-J transitions, and equal to a rotational temperature, $T_{\rm rot}$. This assumption could be rough in some cases but is useful to derive physical parameters from the observations and the calculated values can be easily scaled if one wants to change the assumed excitation state. In the case of CO, that has a low permanent electric dipole moment, the probable thermalization by collisions would ensure the existence of a single rotational temperature. From our data we find that the rotational temperature does not practically vary along the axis. This can be seen in Fig. 6. In this figure we show that the ^{13}CO 2−1/1−0 main-beam temperature ratio in the different velocity ranges remains practically constant with a value $\sim$ 2.8. Since the clumps at the different velocities are practically unresolved in this source we must take into account the beam size and the spatial extent of the source to obtain the brightness temperature ratio. Assuming an extent of the CO clumps of about 6″ (see Sects. 1 and 3), we get that the ^{13}CO 2−1/1−0 brightness ratio is $\sim$ 1.1 in agreement with the ^{13}CO opacities given above; see a similar discussion by Bujarrabal et al. (1997). A similar value is obtained if we take the ^{12}CO line ratio as estimator of the relative dilution factor at both frequencies (since ^{12}CO is probably optically thick). Following the general discussion and calculations by Bujarrabal et al., this ratio indicates that the rotational temperature has a low value, $\sim$ 10 K. Note that the deduced value of the rotational temperature would be even lower if we assume a smaller extent for the emitting region. Those authors also find a low excitation temperature ($\lesssim$ 15 K) in M1-92, an O-rich PPN in many respects comparable to OH 231.8, particularly in its CO emission. The calculated rotational temperature would be an underestimation if the lines are optically thick, but we note that for the typical opacities deduced in the above paragraph a weak effect is expected in the determination of the rotational temperature and values of $T_{\rm rot} \lesssim$ 15 K are still calculated.

With the above assumptions and for a given ^{13}CO abundance, we can calculate the total mass of the clumps (Sect. 4.2). These values of the mass will be used to estimate the abundances of the other molecules. For such a purpose, we will further assume that their lines are optically thin and that the level excitation can be described by a single rotational temperature, that we take to be the same as for CO, $\sim$ 10 K. The low opacity assumption could be wrong in some cases, particularly for the HCN emission, which would lead to an underestimation of the molecular abundance. However, the fact that the emission from other molecules than CO is never significantly stronger than that of ^{13}CO (for a given wavelength) suggests that their opacities are not much larger than those of ^{13}CO. The derived abundances can be easily scaled from our results if we assume a different rotational temperature. We so obtain a first estimation of abundances in the nebula, but we must keep in mind that a deeper analysis of the excitation of the different molecules could be useful to improve the determination of the abundances.

4.2. Clumps in OH 231.8: mass and momentum

We have computed the mass of the clumps in OH 231.8 from our ^{13}CO J=1−0 data taking into account the assumptions in Sect. 4.1 and a distance to the source of 1.5 kpc (a previous estimation of this mass from ^{12}CO data can be seen in Alcolea et al. 1996). For this molecule, we suppose a relative abundance X(^{13}CO) (= ^{13}CO/H_2 abundance ratio) of 2 10^{-5} (see Bujarrabal et al. 1997). ^{13}CO data for the southern clump with the extreme positive velocity (I6 velocity range) was found to be too noisy to calculate its mass properly. Then we have made our calculations for this velocity range from the ^{12}CO 1−0 maps assuming a relative abundance X(^{12}CO) of 2 10^{-4}. This value

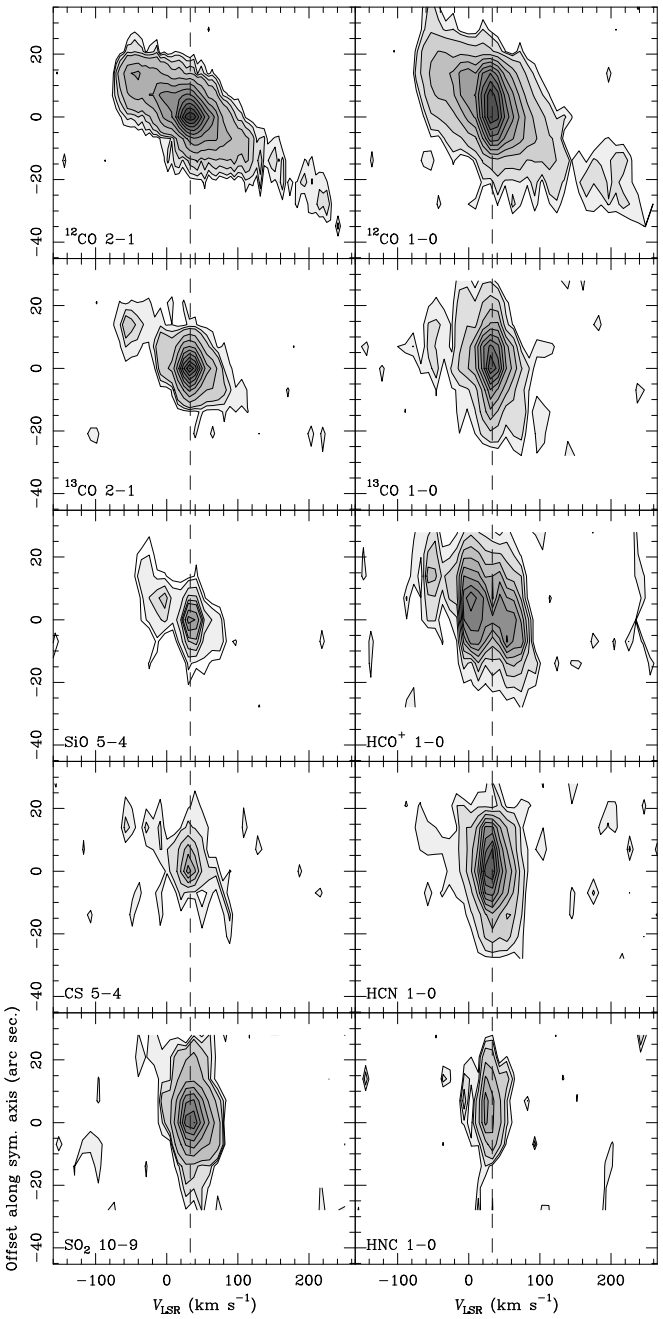

Fig. 4. Intensity as a function of velocity and position along the symmetry axis of the observed lines. For the different transitions, contours in percentage of the maximum (see values in Fig. 1) are, ^{12}**CO 2-1**: 2.5, 4, 6.5 and 10 to 100 by 10; ^{13}**CO 2-1**: 3, 6.5 and 10 to 100 by 10; **SiO**: 5, 10, 20, 30, 40 and 50 to 100 by 20; **CS**: 5 and 10 to 100 by 20; **SO$_2$**: 1.5, 3, 4.5 and 10 to 100 by 15; ^{12}**CO 1-0**: 3, 5 and 10 to 100 by 10; ^{13}**CO 1-0**: 6 and 10 to 100 by 10; **HCO$^+$**: 11 to 100 by 10; **HCN**: 5 and 10 to 100 by 10; **HNC**: 15 20 30 to 100 by 20.

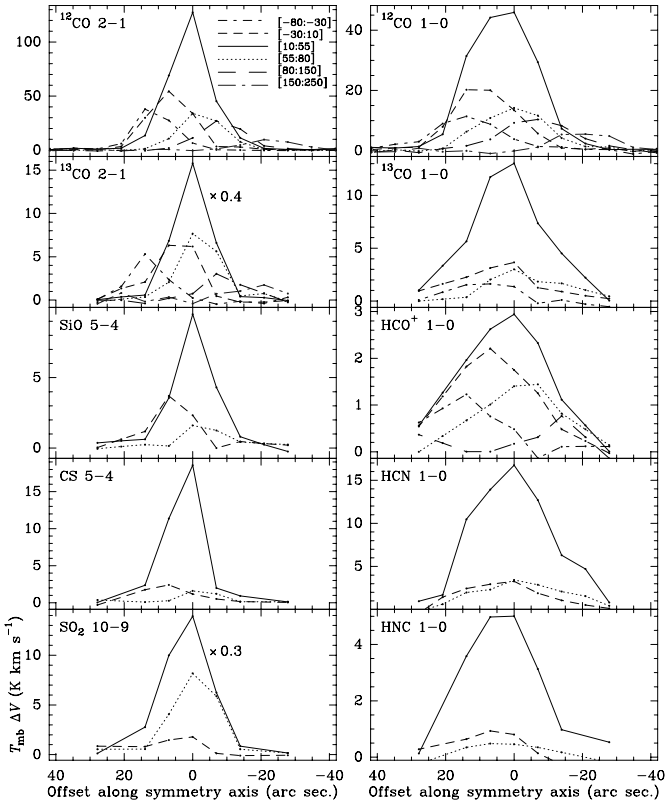

Fig. 5. Integrated intensity in representative velocity ranges along the symmetry axis. The representation of the LSR velocity intervals is indicated in the upper-left panel.

is consistent with the abundance that we would obtain in the I5 velocity range (also in the south lobe) applying to ^{12}CO the procedure described in Sect. 4.1, and also compatible with the CO abundances expected in this kind of objects (see e.g. Alcolea et al. 1996). All the results, presented in Table 1, have been calculated using $T_{\rm rot}$ = 10 K. However we have also made calculations with values of $T_{\rm rot}$ = 5 and $T_{\rm rot}$ = 15 K (as we have mentioned, temperatures higher are improbable). The value of the mass contained in the nebula that we find in this two cases is higher than the obtained value using $T_{\rm rot}$ = 10 K. Nevertheless, variations greater than 20% have not been found. As we see in Table 1, a total mass of $\sim 0.5\ M_\odot$ is calculated for the whole nebula. Approximately the 58% of the molecular mass is contained in the central component, and the 23% and 19% are distributed in the north and south lobes, respectively.

There are however indications of that we are underestimating the actual mass. We have already discussed (see Sect. 4.1 and previous paragraph) that some underestimation in the mass calculation can be produced due to opacity effects and an erroneous assumed temperature, mainly for the central component. Moreover, the mass in dust grains deduced for this nebula (Kastner et al. 1995) is very large, $\sim 0.01\ M_\odot$; since the typical gas/dust mass ratio in these evolved objects is about 100, we expect a total mass somewhat larger than our estimation, $\sim 1\ M_\odot$. Finally, we know that photodissociation begins to take place in

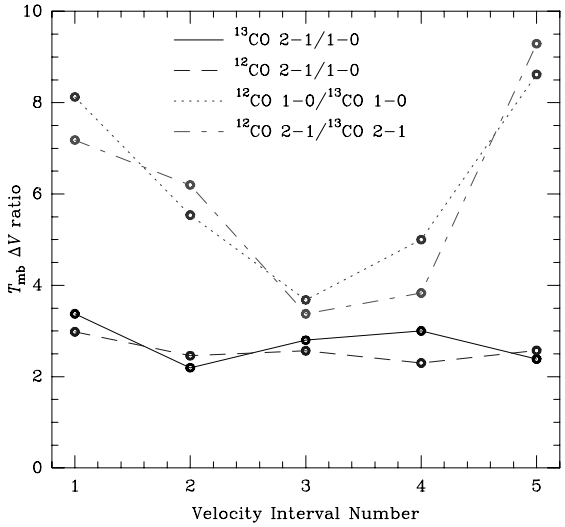

Fig. 6. Ratio of the integrated intensity in representative velocity ranges, I1 to I5, for ^{12}CO and ^{13}CO transitions. The meaning of the different dashes is indicated in the top of the figure.

Table 1. Mass, average (deprojected) velocity with respect to the systemic velocity, V_i, and momentum associated to different spectral intervals.

	interval km s^{-1} (LSR)	mass ($M_\odot$)	V_i (km s^{-1})	momentum ($M_\odot$ km s^{-1})
I1	−80:−30	0.033	137	4.5
I2	−30:+10	0.084	67	5.6
I3	+10:+55	0.295		
I4	+55:+80	0.061	54	3.3
I5	+80:+150	0.027	128	3.4
I6	+150:+250	0.010	260	2.6

the PPN phase destroying a large fraction of the molecules in the envelope, even ^{12}CO and ^{13}CO. Then the standard value of the ^{13}CO abundance that we have assumed could be an overestimation of the real one. This fact obviously gives place to a higher value of the calculated mass. However, we do not think that the molecular masses can exceed by more than a factor two those given here, since 1 $M_\odot$ is similar to the mass value given from grain emission measurements and because it is already high for the mass ejected by an object of this kind (see discussion by Alcolea et al.).

The mass results presented in this paper are comparable to those given by Alcolea et al. (1996). However, our data indicate now a greater amount of molecular material in the lobes. The total mass flowing axially practically equals the mass in the central clump. We think that our new mass estimations from ^{13}CO data are better than the previous ones, from ^{12}CO observations, due to the uncertain correction for opacity in the ^{12}CO lines. Note also that the slightly lower rotational temperature assumed here has a more reliable empirical basis.

Once we have the mass of the clumps, we can calculate the momentum associated to these different regions of emitting gas. We have calculated the flow velocity taking into account the inclination of the polar axis with respect to the plane of the sky, 40° (Sect. 1), and assuming a systemic velocity of 33 km s^{-1}. The results are shown in Table 1. We find differences smaller than 10% between the momentum driven by the north and south lobes, since the larger velocity in the southern lobe is compensated by a smaller mass. These results are consistent with the actual ideas of post-AGB evolution, which suppose that the momentum of the post-AGB fast wind and the momentum transfer rate to the AGB shell is the same in both lobes (Sect. 5).

From the mass and velocity distribution given here we can also estimate the mass loss rate that originates, during the past AGB phase, the actual molecular envelope of OH 231.8 and the time spent in the post-AGB phase by this source, following the procedures described by Alcolea et al. (1996). Since the numerical values to be used are similar to those obtained by these authors, we just confirm their results, i.e. a past mass loss rate $\gtrsim 10^{-4}$ $M_\odot$ yr^{-1} and a post-AGB time of about 1000 yr.

4.3. Molecular spatial distribution

Following the procedures explained in Sect. 4.1 and taking into account the total mass of the clumps obtained from the ^{13}CO data (see Sect. 4.2; note that, therefore, the calculated molecular abundances depend on the assumed relative abundance of CO) we have calculated the molecular abundances of the observed species (excepted ^{12}CO, the emission of which may be optically thick). We present these results in Table 2.

We note from these results the approximately constant abundance along the whole nebula of HCN, HNC, and CS, that may be slightly more abundant in the central core (which could also be due to a weak opacity effect in the ^{13}CO emission and therefore to a slight underestimation of the mass of the central clump). It is also remarkable that the north lobe has a significantly larger SiO abundance than the south lobe; the opposite is found for SO_2. Note that such an asymmetry in the SiO and SO_2 abundances can be directly inferred from the intensity distributions (Figs. 1, 4) and that it cannot be due to excitation effects, since for both lines the levels are placed at a similar high energy from the ground.

The most interesting result from these calculations is the very strong decrease in the central clump of the HCO^+ abundance, that is about three times lower than in the outer parts of the nebula. Also in this case, the behavior of the abundance is expected from the direct measurements. As discussed in Sects. 3 and 5 this effect cannot be explained invoking selfabsorption nor excitation effects. In general, the HCO^+ intensity is found to be particularly high, as happens for other PPNe and PNe and contrarily to the case of the AGB envelopes, where HCO^+ emission is very weak and its abundance is thought to be very low. This relatively high HCO^+ abundance in PPNe could be due either to shock induced or to photon dominated chemistries (Cox et al. 1992). Our results suggest that the efficient formation of this molecule in OH 231.8 is due to shock chemistry, since the HCO^+ emission appears particularly intense in the shock-accelerated lobes, and not in the clump close to the star where one expects

Table 2. Calculated molecular abundances in the different clumps associated to the different velocity ranges (LSR).

Velocity range (km/s)	X(HCO^+)	X(SiO)	X(HNC)	X(HCN)	X(CS)	X(SO_2)
−80:−30	$1.9\ 10^{-8}$	$1.1\ 10^{-8}$	$0.7\ 10^{-8}$	$5.0\ 10^{-8}$	$0.7\ 10^{-7}$	
−30:+10	$1.4\ 10^{-8}$	$2.3\ 10^{-8}$	$1.3\ 10^{-8}$	$4.7\ 10^{-8}$	$0.4\ 10^{-7}$	$0.3\ 10^{-5}$
+10:+55	$0.5\ 10^{-8}$	$1.7\ 10^{-8}$	$2.1\ 10^{-8}$	$6.9\ 10^{-8}$	$0.8\ 10^{-7}$	$1.4\ 10^{-5}$
+55:+80	$1.3\ 10^{-8}$	$1.5\ 10^{-8}$	$0.9\ 10^{-8}$	$6.8\ 10^{-8}$	$0.3\ 10^{-7}$	$1.4\ 10^{-5}$
+80:+150	$1.5\ 10^{-8}$	$1.2\ 10^{-8}$	$1.1\ 10^{-8}$	$2.6\ 10^{-8}$	$0.4\ 10^{-7}$	$1.4\ 10^{-5}$
+150:+250	$< 2.5\ 10^{-8}$	$\lesssim 1.0\ 10^{-8}$			$< 1.0\ 10^{-7}$	

the maximum photoionization rate. On the other hand, Cox et al. conclude that the high HCO^+ abundance also deduced for another PPN, CRL618, is due to photochemistry, based on the relatively low wing/core intensity ratio observed in this source. We note that these diverging conclusions are difficult to avoid since they are directly based on the different properties of the observed HCO^+ spectra in these sources, that are indeed quite different objects. The axial distortion in the molecular envelope of CRL618 is slight and the flow occupies a tiny region, moreover, CRL618 is carbon rich.

Our molecular abundances are somewhat lower than those derived by Morris et al. (1987) for the whole nebula. The discrepancy is mainly due to the different value of the total mass or, equivalently, of the ^{13}CO abundance. In Morris et al. the ^{13}CO relative abundance is quite high, 10^{-4}, and subsequently the total mass is lower than ours. We also note the difference between the rotational temperature assumed in both works (Morris et al. assumed a rotational temperature equal to 25 K), which mainly affects the abundance determination for SO_2, since we observed a relatively high-excitation line for this molecule. In both works, the rotational temperature has been obtained from observational data, but our observations (ten years after) are significantly more accurate and take into account the different parts of the nebula. We also note that Morris et al. only derive average values for the whole nebula, contrarily to our results that include information about the chemical variations across the nebular axis.

5. Conclusions

We have mapped the protoplanetary nebula OH 231.8+4.2 (OH 231.8) in mm-wave lines of ^{12}CO(1-0 and 2-1), ^{13}CO(1-0 and 2-1), SiO (5-4), CS (5-4), SO_2 ($10_{0,10}$-$9_{1,9}$), HCO^+ (1-0), HCN(1-0), and HNC(1-0). See central position spectra and the total CO extent in Figs. 1 and 2. The molecular envelope of OH 231.8 is comparable in extent to the optical image. All the observed molecules share the strong velocity gradient found in CO (Alcolea et al. 1996), see Figs. 3 and 4. CO shows the largest total spatial and velocity extent, as expected in view of its high intensity. The southern lobe is clearly more extended and shows the highest flow velocity that, after deprojection (Sect. 3), reaches a value relative to the central core as high as 330 km s^{-1}.

The structure of the spatial and kinetic extent of the observed molecules, except for HCO^+, is similar to that of CO (Figs. 4 and 5). A central clump at the central velocity (around 33 km s^{-1} LSR) dominates the emission, and the line wings extend along the nebula axis. The redshifted emission comes from the extended southern lobe and the blueshifted one originates in the northern more compact lobe, which is known to point toward us from optical data (Sect. 1). This high-velocity axial flow (that is also observed in other PPNe, the best example being M1-92, e.g. Bujarrabal et al. 1997) seems to be due to the interaction between fast, bipolar post-AGB jets and the dense, mostly isotropic shell ejected during the past AGB mass-loss process. The fast jet is expected to impinge on polar regions of the dense (slow) shell communicating a significant amount of momentum to a good deal of this shell, probably by means of a bow-like shock. The central condensation of OH 231.8 shows a velocity dispersion of about 45 km s^{-1} and seems to be a (probably toroidal) clump that is weakly affected by the wind interaction.

It is also remarkable the clumped structure of the molecular envelope of OH 231.8. The nebula seems to be formed by a number of different components, although they show some continuity in the velocity-position diagram and do not separate from the velocity gradient mentioned above. (For simplicity in our calculations, we have divided OH 231.8 in six clumps, associated to six velocity ranges, I1 to I6, see Sect. 3, Fig. 2.)

This strong velocity gradient observed in OH 231.8 is expected from quite general (and robust) dynamical considerations (see Shu et al. 1991). The shells ejected by AGB stars are thought to show a strong density variation with the radius, proportionally to $1/r^2$. If (a part of) such a shell is accelerated by interaction with a bipolar jet, the outer layers produce on it a ram pressure that increases with the velocity of the shocked region, up to compensate the ram pressure of the wind interaction. From this point, both forces are expected to vary proportionally to $1/r^2$, and then the velocity must be kept constant. Even if the balance is not perfect, the decrease of the forces with the distance to the star implies that the velocity must reach soon a final value. This means that during most of the path travelled by the accelerated clumps the velocity is approximately the same for each one (but probably not the same from one clump to another). If the interaction started at about the same time for all the clumps, the constant-gradient law must hold.

HCO^+ shows a peculiar velocity-position distribution of flux. There is an intensity relative dip at the central core; the most intense emission comes from clumps displaced towards both

lobes, showing the velocity shifts that correspond to the well established velocity gradient. This result cannot be explained invoking selfabsorption, since in expanding envelopes selfabsorption just appears at relatively negative velocities (Sect. 3; this property of selfabsorption is for instance observed in the HCO^+ line from the PPN CRL618, Cernicharo et al. 1989). Moreover, the weak HCO^+ intensity strongly suggests optically thin emission. Excitation effects cannot easily explain neither this peculiar HCO^+ distribution, since the J=1−0 line is difficult to excite and one would expect the most intense emission to take place in the dense central part of the nebula. Therefore, we conclude that this peculiar flux distribution is probably due to an actual increase of the HCO^+ abundance towards the lobe regions that have suffered a strong (shock) acceleration. As discussed in Sect. 4.3, this result suggests that HCO^+ is efficiently formed in OH 231.8 by shock chemistry.

We have calculated for the six clumps the total mass and the molecular abundances. The mass is calculated from the ^{13}CO data, after estimating the excitation state of this molecule, which is found to be almost constant across the nebula and equivalent to a rotational (and kinetic) temperature $\sim$ 10 K (Sect. 4.2, Table 1). For the other molecules we also assume that the excitation of the low-J levels can be described by a single rotational temperature (Sect. 4). The resulting abundances (Table 2, Sect. 4.3) confirm, in particular, the high HCO^+ abundance in the nebula lobes. We also note the different behavior of SiO and SO_2: while SiO is clearly more abundant in the northern lobe, the SO_2 abundance is larger in the south (we also argue that this result is probably not related to excitation effects, which are expected to be similar in both cases). The fact that SiO is observed in the axial flow at large distances from the star (contrarily to the case of AGB envelopes, in which SiO is only found very close to the star) also indicates that shock-induced chemistry is efficient in the OH 231.8 lobes, in this case extracting molecules from dust grains (see discussion on SiO abundance in molecular flows by Bachiller 1996). The molecular abundances given here are in general lower than those obtained by Morris et al. (1987). We argue (Sect. 4.3) that our abundance determination represents a significant improvement with respect to previous results, because of our better observational data, including mapping, and a more reliable model for the distribution of excitation and density across the nebula.

The calculated values of the total mass and momenta of the different clumps are given in Table 1; as discussed in Sect. 4, they can be somewhat underestimated but probably by no more than a factor 2. The total mass of the molecular envelope is very large, probably between 0.5 and 1 $M_\odot$. Note that at least 0.2 $M_\odot$ have been accelerated in the axial direction by more than 40 km s^{-1}. We find that the northern lobe is about 20% more massive than the southern one, but that their total momenta are almost the same (within less than 10%), due to the highest velocities in the southern lobe. This is in agreement with theoretical explanations of the peculiar optical appearance of OH 231.8 (the Calabash Nebula). Icke and Preston (1989) have proposed that the shape in the visible of the OH 231.8 can be explained if the bipolar post-AGB jet has communicated almost the same momentum to both lobes, but the northern one is slightly more massive. In such a case, the light lobe must attain a larger velocity and a wider structure; in order to explain the observations, their calculations require that the northern lobe is about 30% more massive.

It is believed that the mass loss in AGB stars is driven by the pressure exerted by the stellar radiation on the envelope material; in our case the situation is different because of the high measured momenta. As we have mentioned, the high-velocity molecular material was probably accelerated by a short-duration interaction with the bipolar post-AGB wind. Since the total post-AGB time is probably $\sim$ 1000 yr, the wind interaction process would have lasted $\lesssim$ 100 yr in order to explain the constant velocity gradient. We calculate from our results that during this time period the molecular gas won an energy $\sim$ 2.2 10^{46} erg and a momentum $\sim$ 3 10^{39} gr cm s^{-1}. For a stellar luminosity $\sim$ 10^4 $L_\odot$, the above total energy is released by stellar radiation in about 17 yrs, therefore the conversion from radiative to kinetic energy does not need to be anomalously efficient to explain the observations. However, the momentum per year of the stellar radiation is equivalent to 4 10^{34} gr cm s^{-1} yr^{-1}. Therefore, more than 70000 yr would have been necessary to power the observed outflow by radiation pressure: the radiation momentum is too low to explain the momentum of the molecular outflow by at least a factor 700. The situation is worse if we take into account the high collimation of the material outflow, which is not expected for radiation.

The conversion factor from radiative to kinetic momentum (due to photon pressure acting onto dust grains) can be somewhat larger than one (but not much larger than 10) due to multiple scattering (e.g. Netzer and Elitzur 1993); such an effect helps to understand the very copious mass loss in the last AGB phases but, as we see, it is still unable to explain the high axial momentum presently measured in OH 231.8. Even if we assume that the wind interaction is taking place during the whole post-AGB time (about 1000 yr), the disagreement persists. Errors in the mass values also seem unable to explain this problem. As we have mentioned, the assumptions we have made in the mass calculation (low excitation temperature, relatively high ^{13}CO abundance, optically thin emission) should always lead to an underestimation of the mass. If the distance we assumed is wrong, this would affect in the same way the calculation of the kinetic momentum and of the stellar luminosity, the radiation/mass momentum ratio being unchanged. Errors in the assumed inclination of the nebula axis can produce at most an overestimation of the velocity by a (moderate) factor $\sim$ 1.5. We conclude that the high kinetic momentum in the axial direction of the molecular clumps has not been radiatively released by the star. We note that the situation in OH 231.8+4.2 is quite similar to that often present in bipolar outflows from young stars, except for that we cannot invoke here momentum transfer from interstellar material accretion. We speculate that the needed momentum was ejected by the central star of OH 231.8 by another mechanism, like the conversion of gravitational energy of the binary system (in the case the star is multiple, Sect. 1) or the ejection of material during a peculiar phase of stellar pulsation.

Acknowledgements. We remain grateful to Hans Olofsson for calling our attention, several years ago, on the existence of a velocity gradient in this source. Also we wish to thank to Michel Guélin for fruitful comments on the outflow energy. This work has been partially supported by DGICYT, project number PB 93-0048.

References

Alcolea J., Bujarrabal V., Sánchez-Contreras C., 1996, A&A 312, 560
Bachiller R., 1996, ARA&A 34, 111
Bowers P.F., Morris M., 1984, ApJ 276, 646
Bujarrabal V., Alcolea J., Neri R., Grewing M., 1997, A&A 320, 540
Cernicharo J., Guélin M., Martín-Pintado J., Peñalver J., Mauersberger R., 1989, A&A 222, L1
Cohen M., Dopita M.A., Schwartz R.D., Tielens A.G.G.M., 1985, ApJ 297, 702
Cohen M., 1981, PASP 93, 288
Cox P., Omont A., Huggins P., Bachiller R., Forveille T., 1992, A&A 266, 420
Icke V., Preston H.L., 1989, A&A 211 409
Kastner J.H., Weintraub D.A., Zuckerman B., Becklin E.E., McLean I., Gatley I., 1992, ApJ 398, 552
Kastner J.H., Weintraub D.A., 1995, AJ 109(3), 1211
Morris M., Bowers P.F., Turner B.E., 1982, ApJ 259, 625
Morris M., Guilloteau S., Lucas R., Omont A., 1987, ApJ 321, 888
Netzer N. and Elitzur M., 1993, ApJ 410, 701
Omont A., Lucas R., Morris M., Guilloteau S., 1993, A&A 267, 490
Reipurth B., 1987, Nature 325, 787
Shu F.H., Ruden S.P. Lada C.J., Lizano S., 1991, ApJ 370, L31
Shure M., Sellgren K., Jones T.J., Klebe D., 1995, AJ 109, 721
Ukita N. and Morris M., 1983, A&A 121, 15

This article was processed by the author using Springer-Verlag LaTeX A&A style file *L-AA* version 3.